

# BEVLM: Distilling Semantic Knowledge from LLMs into Bird’s-Eye View Representations

Thomas Monninger<sup>1,\*</sup>, Shaoyuan Xie<sup>2,\*†</sup>, Qi Alfred Chen<sup>2</sup>, and Sihao Ding<sup>1,⊠</sup>

<sup>1</sup> Mercedes-Benz Research & Development North America, San Jose, USA

<sup>2</sup> University of California, Irvine, USA

{thomas.monninger, sihao.ding}@mercedes-benz.com

{shaoyux, alfchen}@uci.edu

**Abstract.** The integration of Large Language Models (LLMs) into autonomous driving has attracted growing interest for their strong reasoning and semantic understanding abilities, which are essential for handling complex decision-making and long-tail scenarios. However, existing methods typically feed LLMs with tokens from multi-view and multi-frame images independently, leading to redundant computation and limited spatial consistency. This separation in visual processing hinders accurate 3D spatial reasoning and fails to maintain geometric coherence across views. On the other hand, Bird’s-Eye View (BEV) representations learned from geometrically annotated tasks (*e.g.*, object detection) provide spatial structure but lack the semantic richness of foundation vision encoders. To bridge this gap, we propose **BEVLM**, a framework that connects a spatially consistent and semantically distilled BEV representation with LLMs. Through extensive experiments, we show that BEVLM enables LLMs to reason more effectively in cross-view driving scenes, improving accuracy by 46%, by leveraging BEV features as unified inputs. Furthermore, by distilling semantic knowledge from LLMs into BEV representations, BEVLM significantly improves closed-loop end-to-end driving performance by 29% in safety-critical scenarios.

**Keywords:** Autonomous Driving · Large Language Models · Bird’s-Eye View

## 1 Introduction

Large Language Models (LLMs) have rapidly advanced in scene understanding and reasoning [1, 11, 70, 81], attracting growing interest for autonomous driving applications [29, 49, 56, 60, 64, 68]. Integrating language foundation models into autonomous driving systems provides a path towards commonsense reasoning, open-world understanding, and enhanced interpretability, capabilities often

---

(\*) Equal contribution, the order was determined alphabetically.

(†) Work was done during an internship at Mercedes-Benz Research & Development North America.

(⊠) Corresponding author.

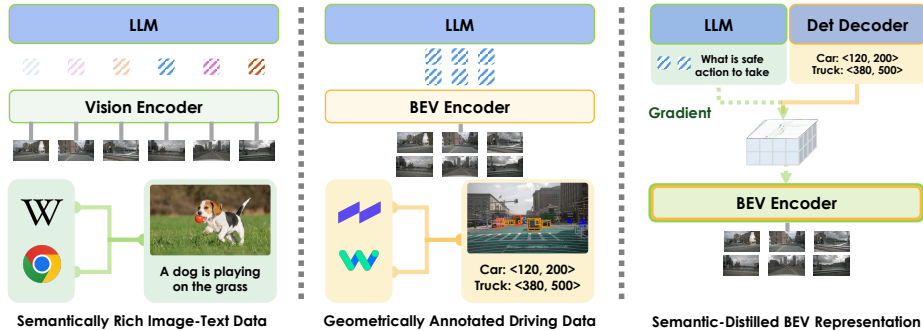


**Fig. 1: Representation Comparison:** Left: Vision encoders can leverage widely available semantically rich image-text data, but process multi-view images independently. Center: Bird’s-Eye View (BEV) encoders provide a spatially consistent scene representation, but are limited to geometrically annotated data. Right (ours): We propose the semantic distillation from LLMs to BEV encoders to build a semantic-enhanced and spatially consistent scene representation.

lacking in conventional perception or end-to-end driving pipelines [73]. Such reasoning ability is particularly critical for handling complex driving scenarios and corner cases, *i.e.*, the “long tail” of the distribution.

To integrate LLMs into autonomous driving, most existing systems leverage Vision Language Models (VLMs) and extract visual tokens independently from multi-view and multi-frame images [27, 29, 53, 55–57, 61, 74, 79]. While this design is straightforward and leverages the large-scale pre-training of VLMs to align vision and language modalities, it introduces two key limitations. As shown in Fig. 1, first, the resulting representations capture each view angle individually and are encoded into different token chunks. This separate processing fails to model spatial consistency, which is crucial for modeling dynamic driving environments [44] and poses a challenge for 3D spatial reasoning of LLMs [19]. Second, this design fails to exploit the temporal correlation, and separate processing makes the computational cost grow proportionally with the number of frames, leading to an inevitable trade-off between capturing long-term temporal information and maintaining computational efficiency [77].

Meanwhile, the Bird’s-Eye View (BEV) representation has become a cornerstone of modern autonomous driving systems [44]. BEV provides a unified top-down view of the 3D environment by fusing information from multiple viewpoints, time steps, and even sensor modalities into a compact and spatially consistent grid. This representation enables more effective reasoning about spatio-temporal relationships among the ego-vehicle, dynamic agents, and static surroundings, which is crucial for reliable scene understanding. Owing to these advantages, the BEV grid has become the de facto intermediate representation for object detection [34, 40], motion prediction [63, 76], and vehicle planning [24, 30].

However, despite its compactness and spatial consistency, the BEV representation cannot be pre-trained at scale using semantically rich image-text datasets, as is possible with foundation visual encoders in VLMs [1, 11, 70, 81]. Large-scale

pre-training is essential for learning transferable visual features that generalize to rare and open-world driving scenarios [52]. The lack of such semantic richness forms a fundamental bottleneck, preventing BEV-based representations from being adopted by the advances of LLMs.

In this paper, we conduct the first rigorous experiments to show the advantages of the spatially consistent BEV representation for LLM reasoning in autonomous driving, which we call **Bird’s-Eye View Language Model (BEVLM)**. Specifically, BEV improves scene understanding accuracy by 46.0% over multi-view inputs and achieves comparable performance to foundation vision encoders with 10× larger model size. Based on the promising results, we argue that BEV should serve as a superior scene representation compared to processing multiple separate images for LLMs. Building on the benefits of the BEV grid, we introduce semantic distillation using the BEVLM framework, a method designed to distill the semantic richness from LLMs into BEV representations. Specifically, we frame the LLM as a fixed semantic teacher that provides supervision signals via VQA tasks. The BEV encoder (student) is distilled to produce features that align with the semantic space defined by the teacher LLM. This results in a semantic-aware BEV encoder that can interact effectively with language models while maintaining spatial structure. This design unifies the strengths of structured 3D world modeling and semantically rich language reasoning and is shown to significantly improve driving safety in the evaluation. Specifically, our framework improves the safety score by 29.0% and decreases the collision rate by 11.3% when evaluated closed-loop in safety-critical scenarios.

Our contributions are summarized as follows:

1. We are the first to carry out a representation study that compares individual multi-frame multi-view perspective images and joint BEV representations for LLM reasoning in autonomous driving.
2. We propose BEVLM, a framework to distill semantic information from LLMs into the BEV encoder while preserving the spatial BEV representation.
3. We train an end-to-end driving model from the distilled BEV encoder and find significant improvements in closed-loop evaluation, confirming distillation performance specifically in safety-critical scenarios.

## 2 Related Work

**LLMs for Autonomous Driving.** With the rapid advancement of LLMs, there is a growing interest in applying their reasoning and knowledge capabilities to autonomous driving. The key motivation is to leverage the human knowledge and commonsense reasoning embedded in LLMs to better handle corner cases and long-tail scenarios [73]. Existing studies generally follow two directions: (1) using LLM-generated text as high-level guidance for BEV-based end-to-end driving pipelines [17, 29, 49, 57, 60, 68]; and (2) directly generating driving trajectories through LLMs [9, 18, 20, 26, 27, 55, 56, 67, 69, 78, 79]. However, most of these approaches still follow the conventional VLM paradigm, where visual features are extracted independently from individual camera views and frames. This design

limits the LLM’s ability to capture spatio-temporal consistency and geometric relationships across views. Recent works [4, 62, 77] begin to explore connecting BEV and language modalities. Yet, a systematic study comparing the representational advantages of image-based versus BEV-based inputs for LLM reasoning has been missing. Also, solutions for addressing the semantic gap between these two representations are still underexplored.

**BEV Representation.** The BEV representation combines and integrates information from multiple views, time steps, and even sensor modalities [44, 65]. It has become a central intermediate representation for full-stack autonomous driving, enabling perception [25, 34, 40, 47, 76], prediction [16, 24, 76], and planning [24, 30]. However, learning semantically rich BEV representations remains an open challenge [45, 72]. Current BEV learning methods rely heavily on dense geometric supervision, often through object detection [34, 40], map construction [36, 46], or joint end-to-end training [24, 30]. While such supervision provides strong geometric cues, it limits the semantic richness needed for understanding complex, safety-critical scenarios, which is an essential requirement for conditional, highly, and fully automated driving systems.

**Safety-Critical Evaluation.** Autonomous driving is inherently a safety-critical task, where unsafe decisions can result in severe consequences [48, 59]. Most existing studies emphasize the robustness of the perception module, particularly under out-of-distribution inputs [32, 65] or adversarial perturbations [7, 54, 66]. In contrast, the safety of the planning module has received relatively limited attention. Recently, several benchmarks have been introduced to assess planning safety [13, 28, 41]. For instance, the NeuroNCAP benchmark [41] generates safety-critical driving scenarios through closed-loop simulation. In this work, we focus on enhancing the semantic understanding of the BEV representation to promote safer decision-making in end-to-end autonomous driving systems.

### 3 BEV Representation for Spatial Reasoning

To understand how BEV representations affect spatial understanding, this section examines whether LLMs can effectively interpret and reason over BEV inputs, and then compares BEV and image-based representations in supporting spatial reasoning. VLMs typically adopt image patch tokenization as input [15] and leverage large-scale pre-training to achieve general semantic understanding [33, 52]. However, such perspective-based representations lack spatial consistency across views, which is essential for reasoning about dynamic driving environments [8, 19]. In contrast, BEV representations provide a unified and geometrically consistent view of the scene but are less semantically rich due to geometry-oriented training data [44]. The results of this study motivate Sec. 4, where we enhance BEV representations with semantic knowledge from LLMs.

**Table 1: BEV Projector Alignment Study.** We compare the performance between the BEV-based detected bounding box and the LLM that directly operates on the same BEV grid. We report binary classification accuracy. *Majority class* denotes using the majority choices from the training set for each category. The final score is averaged across all 10 categories, as we only show the top 5 frequent objects. For full results, please refer to the Appendix B.

Model	Modality	cars	peds.	trucks	cones	barriers	Avg.
Majority class	-	92.7	81.9	65.0	59.6	54.8	78.2
Linear probe	-	94.6	87.2	84.2	83.8	83.9	88.7
Detection <sub>UniAD</sub>	-	91.1	90.9	86.7	<b>99.0</b>	<b>99.6</b>	92.8
InternVL3 <sub>1B</sub>	B <sub>UniAD</sub>	94.7	88.9	85.8	90.1	88.6	90.8
InternVL3 <sub>8B</sub>	B <sub>UniAD</sub>	97.7	<b>94.8</b>	<b>89.7</b>	94.0	95.0	<b>95.3</b>
DeepSeek-VL <sub>1B</sub>	B <sub>UniAD</sub>	<b>95.1</b>	92.0	84.9	92.6	92.2	92.2

### 3.1 BEV-to-Language Alignment

**Research Question 1:** *Can BEV representations be aligned with the language space such that LLMs can reason over them as effectively as task-specific BEV perception modules?*

In this section, we examine whether BEV features can be fully aligned with the language space for LLM-based reasoning. We mainly compare two setups: (1) our BEVLM framework, which uses an LLM receiving BEV features through a learned projector [39], and (2) a task-specific BEV model whose outputs are converted to answers via rule-based logic. By comparing their accuracy in identifying objects in the scene, we can assess whether the BEV-to-language projection retains sufficient spatial information for the LLM to reason over as effectively as the task-specific decoder (e.g., detection head).

**Experimental Setups.** We assess whether the projector effectively aligns BEV features with the language space by comparing three results on binary *object-existence* questions from DriveLM-nuScenes dataset [56]. We train the projector on *perception-related* question-answer pairs and evaluate on questions such as “Is there a moving car in the front left?”. We adopt the BEV encoder from UniAD [24] and the language component of InternVL3-VL [81]. The BEV grid is max-pooled to  $50 \times 50$ , producing 2,500 tokens. The original vision encoder is disabled when BEV tokens are used. We choose the language component of a VLM over a pure text-based LLM since we anticipate better spatial understanding from the cross-modal alignment. Additionally, this setup enables us to conduct comparisons across different modalities (Sec. 3.2). Data examples are provided in Appendix C.1. More implementation details can be found in Appendix A.

**Results.** Tab. 1 reports both overall and class-wise accuracy for the five most frequent object categories. We compare BEVLM against three baselines: (1) a *majority class* prior based on DriveLM-nuScenes training split [56, 64]; (2) a stronger linear probe baseline, implemented as an object-specific linear classifier on max-pooled BEV features of the view specified in the question, to consider the influence of data bias on the learning process; and (3) UniAD’s detection

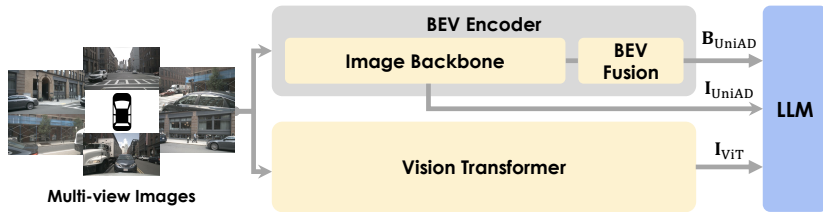


**Fig. 2: Representation Study.** We compare between (1)  $I_{ViT}$ , visual tokens extracted from the Vision Transformer of the original VLM; (2)  $I_{UniAD}$ , visual tokens from the backbone before the BEV fusion; and (3)  $B_{UniAD}$ , BEV tokens produced from the same backbone after the BEV fusion. The input language question is the same, but not visualized here for simplicity.

head, where answers are derived by matching *class*, *moving state*, and *view angle* to the detector outputs. BEVLM substantially outperforms the majority-class and linear probe baselines across all categories, with especially strong gains on more balanced classes such as trucks, cones, and barriers (near 90%). This indicates that the projector is not simply capturing dataset priors but preserving meaningful spatial and semantic cues for LLMs to answer correctly.

BEVLM also approaches the accuracy of UniAD’s task-specific decoder. Specifically, InternVL3<sub>1B</sub> achieves 90.8% and DeepSeek-VL<sub>1B</sub> achieves 92.2%, versus UniAD’s 92.8%. Scaling the InternVL3 to 8B yields 95.3%, surpassing the detector itself. These results show that a simple MLP projector can effectively map BEV features into the language space. Complete results are in Appendix B.

### 3.2 Comparative Study of Visual Representations

**Research Question 2:** *Are BEV representations more effective than perspective-view inputs for enabling LLMs to perform spatial reasoning?*

Building on the successful BEV-to-language alignment, we next compare different visual representations to examine which one better supports spatial reasoning. Specifically, we evaluate three setups, shown in Fig. 2: (1)  $I_{ViT}$ , visual tokens from the ViT of the original VLM [81]; (2)  $I_{UniAD}$ , tokens from UniAD’s image backbone before BEV fusion; and (3)  $B_{UniAD}$ , BEV tokens produced after fusing multi-view features into BEV space [24]. This analysis allows us to isolate the advantages of the BEV representation over conventional image-based inputs in capturing geometric and spatial relationships within driving scenes. More implementation details can be found in Appendix A.

**Single-View Reasoning.** We start with DriveLM *object-existence* questions, which are designed for single-view reasoning. The quantitative results are presented in Tab. 2a. We first observe that BEV representations show advantages over multi-view inputs. Additionally, increasing the size of the LLM from 1B to 8B gives a substantial improvement from 89.8% to 94.5% accuracy, showing

**Table 2: DriveLM Results and Generality Analysis.** We report accuracy, precision, recall, and F-1 scores. “I” denotes image-space, while “B” denotes BEV-space. “Proj.” indicates training the MLP projector. Metrics are reported as percentages.

(a) InternVL3 Results							(b) DeepSeek-VL Results						
Models	Mod.	Proj.	Acc.↑	Prec.↑	Recall.↑	F1↑	Models	Mod.	Proj.	Acc.↑	Prec.↑	Recall.↑	F1↑
InternVL3 <sub>1B</sub>	I <sub>ViT</sub>		74.2	72.2	97.7	83.0	DS-VL <sub>1B</sub>	I <sub>ViT</sub>		61.5	84.1	49.8	62.6
InternVL3 <sub>1B</sub>	I <sub>ViT</sub>	✓	90.3	90.0	95.5	92.7	DS-VL <sub>1B</sub>	I <sub>ViT</sub>	✓	85.3	86.5	91.5	89.0
InternVL3 <sub>1B</sub>	I <sub>UniAD</sub>	✓	89.8	90.1	94.6	92.3	DS-VL <sub>1B</sub>	I <sub>UniAD</sub>	✓	90.4	89.9	97.3	93.5
InternVL3 <sub>8B</sub>	I <sub>UniAD</sub>	✓	94.5	94.6	97.0	95.8	DS-VL <sub>1B</sub>	B <sub>UniAD</sub>	✓	92.2	90.5	98.2	94.2
InternVL3 <sub>1B</sub>	B <sub>UniAD</sub>	✓	90.8	90.3	96.1	93.1							
InternVL3 <sub>8B</sub>	B <sub>UniAD</sub>	✓	95.2	95.2	97.7	96.4							

**Table 3: Ego3D Results.** We evaluate cross-view reasoning question types (i.e., “object-centric” in Ego3D) and report accuracy for Multiple-Choice-Question (MCQ) and L1 error for numerical distance estimation. We use the InternVL3<sub>1B</sub> as the LLM. “Enc. Size” and “#Token” denote the visual encoder size and the number of visual tokens, respectively. Token number details can be found in Appendix A.3.

Modality	Enc. Size	#Token	MCQ Accuracy (%) ↑				L1 (m) ↓	
			Loc.	Abs-Dist.	Rel-Dist.	Avg.	Dist	
I <sub>ViT</sub>	400M	4,608	13.95	23.81	52.94	28.57	14.15	
I <sub>ViT</sub> w/ ft.	400M	4,608	<u>60.47</u>	<b>50.00</b>	<b>79.41</b>	<b>62.18</b>	<u>7.42</u>	
I <sub>UniAD</sub>	40M	2,250	39.53	26.19	64.71	42.02	9.01	
B <sub>UniAD</sub>	44M	2,500	<b>67.44</b>	<u>45.24</u>	<u>73.53</u>	<u>61.34</u>	<b>7.05</b>	

that a more powerful LLM can better utilize relevant information from the token space. The 1B LLM processing tokens from B<sub>UniAD</sub> achieves 90.8% accuracy, which outperforms both I<sub>ViT</sub> (90.3%) and I<sub>UniAD</sub> (89.8%). This confirms the hypothesized benefits of the BEV representation. Also here, using the larger 8B LLM yields a substantial improvement to 95.3% accuracy, outperforming the equivalent model on I<sub>UniAD</sub>. Similarly, DeepSeek-VL<sub>1B</sub> shows the same trend where the B<sub>UniAD</sub> surpasses the I<sub>ViT</sub> and I<sub>UniAD</sub>.

Therefore, even in the context of single-view reasoning tasks, our empirical findings indicate that the BEV representation exhibits a consistent advantage over perspective-view counterparts. This observation motivates a more rigorous investigation into the representation gap when subjected to the demands of complex, cross-view spatial reasoning.

**Cross-View Reasoning.** The advantage margin of BEV representation is limited in the DriveLM dataset mainly due to the single-view reasoning questions. Therefore, we show the results on the cross-view reasoning Ego3D dataset [19]. Specifically, we focus on the *object-centric* questions, which ask about the spatial relationship between two objects in different ego camera views. Therefore, the LLMs are required to reason over the entire driving scene beyond a single view as in DriveLM perception data. As shown in Tab. 3, we find the BEV representation surpasses the perspective-view representation by a noticeable margin.

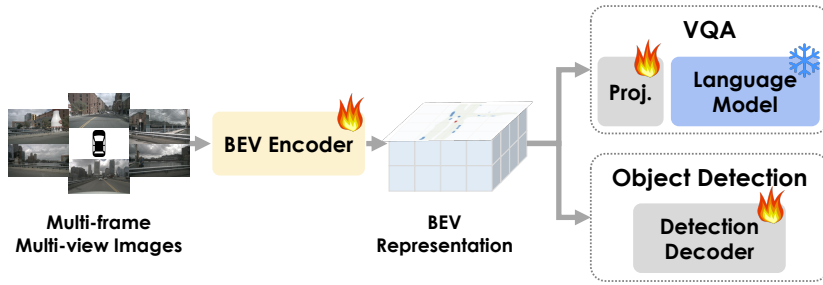


**Fig. 3: BEV Semantic Distillation:** We distill the knowledge from the language model to the BEV representations by using Visual Question Answering (VQA) tasks while regularizing BEV spatial structure using the original object detection tasks.

Specifically, the MCQ accuracy is improved by 46.0%, and the L1 error is decreased by 27.8%. Additionally,  $B_{\text{UniAD}}$  shows comparable performance to  $I_{\text{ViT}}$  w/ ft. even though the ViT encoder is  $10\times$  larger. The results further confirm the advantages of BEV representation for complex spatial reasoning. Data examples are provided in Appendix C.2.

One concern is that the BEV fusion introduces extra parameters (e.g., spatial attention [34]), confounding comparisons between  $B_{\text{UniAD}}$  and  $I_{\text{UniAD}}$ . However, we argue this impact is minor as (1) the module size is only 10% of the backbone [21], and (2)  $B_{\text{UniAD}}$  shows comparable performance to  $I_{\text{ViT}}$  despite the ViT model size being an order of magnitude larger. Thus, the gains mainly stem from BEV’s representational advantages rather than added capacity. Therefore, we can conclude that BEV representation significantly improves the LLM’s spatial reasoning capability, especially for panoramic scene understanding.

## 4 BEVLM for Semantic Distillation

**Research Question 3:** *Can we enhance the semantic awareness of BEV representations, and thereby improve driving safety, by distilling commonsense knowledge from LLMs into BEV encoders?*

The representation study in Sec. 3.2 confirmed that BEV tokens show superior spatial consistency and geometric coherence compared to perspective-view image tokens for enabling better LLM spatial reasoning. However, BEV encoders are typically trained solely on dense, task-specific, and precise geometric annotations (e.g., bounding boxes [34], map elements [36], or ego trajectories [24]). This training paradigm limits the BEV encoder’s supervision to geometric information, ignoring the broader semantic knowledge and commonsense reasoning essential for safety-critical corner cases. Thus, this paradigm is the key bottleneck that prevents a wide adoption of BEV representations for LLMs in autonomous driving, compared to semantically rich 2D visual representations [55–57, 79].

Therefore, we pioneer the exploration of distilling semantic knowledge from pre-trained LLMs into the BEV encoder. By training the BEV encoder using the

BEVLM framework to perform high-level visual question answering (VQA) [2] on safety-related topics, the encoder is *forced* to capture comprehensive, safety-related aspects of the scenario that cannot be covered by geometric supervision alone. This novel semantic distillation process yields a semantically-enhanced BEV representation that is universally beneficial for downstream tasks, including improved performance in LLM-based reasoning [56] and enhanced planning in end-to-end (E2E) driving systems [24, 30].

In this work, we focus on evaluating the benefits of distilled BEV representations on the E2E driving pipeline. This choice is motivated by the fact that directly relying on LLMs for E2E control (*e.g.*, VLAs) remains challenging due to current issues with real-time efficiency [27, 79] and reliability [14, 64], which are actively being researched. Given that established E2E pipelines [24, 30] remain the most practical architectures for planning, demonstrating improvement in E2E performance provides the most critical evidence of our method’s real-world value. We leave exploring the benefit of a semantically-enriched BEV representation for LLM-based control (*e.g.*, VLAs) as future work.

#### 4.1 BEV Distilled from LLM Semantic Space

As illustrated in Fig. 3, we use a shared BEV representation to support both the VQA and object detection tasks. Unlike output-level distillation [23], our method performs representation distillation [22], where the BEV encoder learns to encode semantic cues directly into its feature grid to satisfy the LLM’s reasoning requirements. Specifically, we frame the LLM as a fixed semantic teacher that provides supervision signals via VQA tasks. The BEV encoder (student) is distilled to produce features that align with the semantic space learned by the teacher LLMs. For example, when the LLM answers a question such as “*What is the safe action for the ego vehicle to take?*”, the BEV tokens *must* encode safety-relevant scene information.

To maintain the spatial structure of the BEV representation, we jointly train with the original perception tasks, such as object detection, which preserve the geometric structure of the BEV grid. This prevents catastrophic forgetting of spatial relationships that are not directly constrained by the distillation.

**Intuitive Interpretation: BEV as a Semantic Manifold.** Unlike standard auxiliary multi-task supervision, where a task-specific head is learned from scratch, we strictly freeze the LLM parameters  $\phi$ . This design choice fundamentally transforms the learning problem: the frozen LLM is no longer a trainable decoder but an *immovable semantic prior*, whose input embedding space defines a fixed, high-dimensional teacher manifold  $\mathcal{M}_{\text{teacher}}$ . The BEV encoder student is therefore forced to reshape its internal feature space to satisfy the structural requirements of  $\mathcal{M}_{\text{teacher}}$ , a qualitatively different objective from simply learning an additional loss term.

We formalize this as *representation distillation via latent alignment*. Let  $\mathcal{X}$  be the input driving scene and  $\mathbf{B}_s = E_\theta(\mathcal{X})$  the BEV feature produced by the student. For a safety-critical query  $\mathbf{q}$ , the frozen LLM’s knowledge base implicitly requires a specific set of ideal semantic token embeddings  $\mathbf{v}^*$  to encode concepts

such as “blocked lane” or “unsafe velocity”, thus to correctly activate its internal reasoning and produce the correct answer  $\mathbf{a}$ . The distillation objective forces the student to align its projected features with  $\mathbf{v}^*$ :

$$\mathcal{L}_{\text{distill}} \approx \|\text{MLP}(E_{\theta}(\mathcal{X})) - \mathbf{v}^*\|_2^2. \quad (1)$$

Since  $\mathbf{v}^*$  cannot be accessed directly, we use the frozen LLM’s cross-entropy loss as a differentiable proxy. Therefore, the VQA dataset is not the end goal, but it acts as an *information bottleneck*: by restricting supervision to complex, reasoning-heavy queries, we selectively distill only the high-level semantics that are absent from the BEV encoder’s geometric training. Thus, both the teacher LLM (studied in Sec. 5.3) and the VQA data (studied in Sec. 5.4) play a critical role in the proposed framework.

## 4.2 Training

Following our previous setup, we use DriveLM-nuScenes [56] as the VQA data for the distillation. We leverage the *full* VQA data, including perception, prediction, behavior, and planning. We also conduct an ablation study for different VQA data types in Sec. 5.4.

We start from the pre-trained BEVFormer checkpoints [34] because UniAD [24] shares the same BEV encoder as BEVFormer and is initialized with the same weights. For the baseline model, we freeze the pre-trained BEV encoder and only train the task-specific decoder. To demonstrate the benefits of our distilled BEV for final E2E driving performance, we introduce this semantic distillation as an additional step after object detection pretraining. The distillation is performed for 1 epoch with equal loss term weights for distillation and object detection. After distillation, we perform the same E2E training as UniAD, freezing the distilled BEV encoder and training all task-specific heads for 20 epochs. Thus, we can study the effects of semantic enhancement on the final E2E tasks. All the experiments are performed on 8 NVIDIA A100 80GB GPUs. Distillation for 1 epoch of the full DriveLM dataset takes  $\sim 35$  h for the 1B and 100 h for the 8B LLM. E2E training time of the UniAD remains unchanged with 115 h.

# 5 Experiments

## 5.1 Experimental Setups

Following UniAD [24], we first evaluate the L2 error on the open-loop nuScenes validation set. Given the observed gap between open-loop and closed-loop evaluation [6, 12, 13, 35], we further evaluate on the closed-loop NeuroNCAP benchmark [41]. NeuroNCAP is a NeRF-based simulation framework, enabling scene reconfigurations and renderings of unseen, safety-critical scenarios.

**Table 4: Open-Loop and Closed-Loop E2E Planning Results.** We compare UniAD performance using the baseline encoder versus the distilled BEV encoder. Open-loop L2 error is measured on nuScenes [5], while NeuroNCAP score and Collision Rate (CR) are measured on the NeuroNCAP benchmark [41].

Method	Training	Open-Loop (nuScenes)				NeuroNCAP	
		L2@1s↓	L2@2s↓	L2@3s↓	Avg.L2↓	Score↑	CR↓
Our Baseline	Det.	0.50	0.99	1.67	1.05	2.10	0.62
Distilled <sub>1B</sub> BEV	Det. + Distill	<b>0.46</b>	<b>0.91</b>	<b>1.55</b>	<b>0.97</b>	2.46	0.63
Distilled <sub>8B</sub> BEV	Det. + Distill	0.48	0.94	1.59	1.00	<b>2.71</b>	<b>0.55</b>

## 5.2 Open-Loop Evaluation

The open-loop E2E results are evaluated on the nuScenes validation set [5]. The results on the L2 error metric at 1 s, 2 s, and 3 s are shown in Tab. 4.

Both distilled models show a clear improvement over the baseline at all time horizons, indicating the potential of BEVLM distillation in reducing the error in imitating human trajectories. However, as shown in prior works [6, 12, 13, 35], open-loop evaluation provides limited signal about real-world performance, especially in safety-critical scenarios. Additionally, the original nuScenes dataset includes scenarios where the ego is mostly moving straight [35, 64]. Therefore, the improvement in closed-loop safety-critical scenarios is not well understood.

## 5.3 NeuroNCAP Closed-Loop Evaluation

To study the closed-loop performance in safety-critical scenarios, we further evaluate the distilled model using the NeuroNCAP benchmark [41]. The benchmark simulates safety-critical scenarios and calculates a NeuroNCAP score between 0 and 5 based on the impact velocity, with 5 being no collision. The NeuroNCAP score provides a more fine-grained evaluation beyond the collision rate metric.

The results are shown in Tab. 4. We show that the UniAD model trained with our BEV encoder after distillation with 1B LLM achieves a substantial improvement with a NeuroNCAP score of 2.46. The collision rate is almost unchanged; hence, the improved NeuroNCAP score highlights a reduction in crash severity. We confirm this by studying the velocity before the collision in Appendix D. Most importantly, our 8B distilled variant reaches an even higher NeuroNCAP score of 2.71, a 10.2% improvement over the 1B variant and a 29.0% improvement over the baseline with no semantic distillation. Furthermore, the collision rate is reduced from 62% to 55%. Thus, the closed-loop evaluation shows a more pronounced improvement for distillation with LLMs, confirming a more nuanced and accurate evaluation compared to the pure open-loop evaluation. The significant improvements in closed-loop evaluation show the benefit of generic semantic distillation compared to geometric supervision, confirming the potential of our methodology for safer autonomous driving. Additionally, the comparison between distillation from 1B and 8B LLMs also illustrates the importance of the

**Table 5: Ablation on BEV Token Downsampling.** Comparison of pooling and lightweight convolutional methods for BEV downsampling. We evaluate across different tasks and metrics (all scores in %). The metric abbreviations are: **B** = BLEU-4 [50], **R** = ROUGE-L [37], **M** = METEOR [3], **C** = CIDEr [58], **Avg.** = Averaged accuracy. We evaluate “Yes” or “No” questions using Accuracy, while other open-ended questions use language metrics. *Max. Pool* achieves comparable accuracy with no added parameters and is used in all experiments.

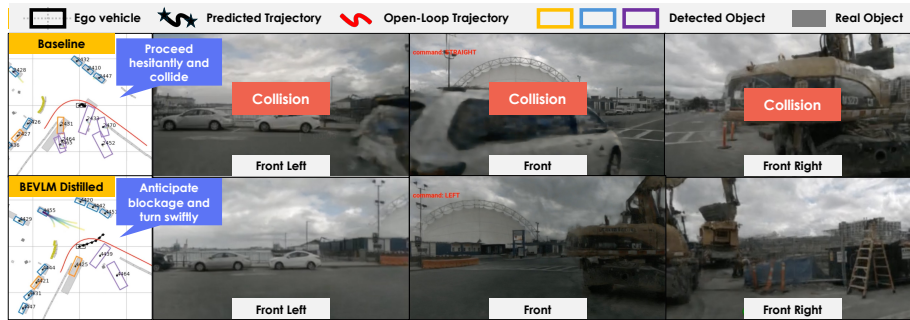
Models	Projector	B↑	R↑	M↑	C↑	cars	peds.	trucks	cones	barriers	Avg.↑
InternVL3 <sub>1B</sub>	Convolution	0.469	<b>0.686</b>	<b>0.610</b>	3.747	94.4	90.0	84.6	86.9	90.4	91.0
InternVL3 <sub>1B</sub>	Depthw. Conv	0.461	0.680	0.604	3.657	94.9	88.2	85.5	89.4	89.3	90.6
InternVL3 <sub>1B</sub>	Concat	0.454	0.673	0.597	3.621	93.8	88.2	86.4	89.4	90.0	90.2
InternVL3 <sub>1B</sub>	Avg. Pool	0.472	<b>0.686</b>	0.609	<b>3.796</b>	94.8	89.1	85.2	89.7	90.8	90.9
InternVL3 <sub>1B</sub>	Max. Pool	0.468	0.682	0.606	3.765	94.7	88.9	85.8	90.1	88.6	90.8
InternVL3 <sub>8B</sub>	Concat	0.468	0.661	0.567	3.521	95.6	91.1	87.3	89.4	91.5	92.4
InternVL3 <sub>8B</sub>	Avg. Pool	0.441	0.627	0.559	3.646	97.2	<b>95.5</b>	<b>91.5</b>	93.6	<b>96.4</b>	<b>95.3</b>
InternVL3 <sub>8B</sub>	Max. Pool	<b>0.485</b>	0.673	0.579	3.703	<b>97.7</b>	94.8	89.7	<b>94.0</b>	95.0	<b>95.3</b>

teacher LLM scale in our proposed pipeline beyond a simple auxiliary VQA task. Specifically, we use the same set of VQA data while observing that scaling the LLMs can further improve the performance.

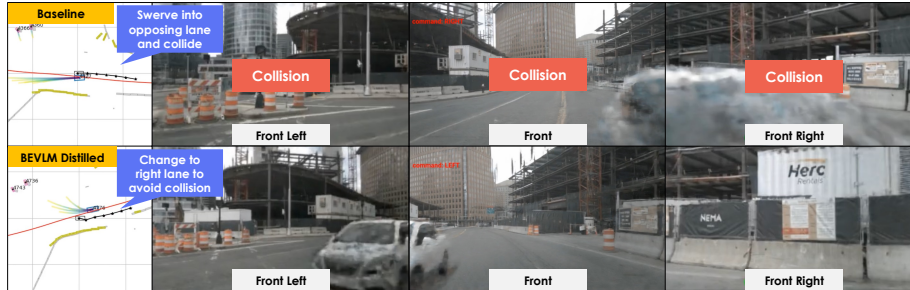
We visualize the results between the baseline model and our distilled version (8B) in Fig. 4. The distilled model consistently demonstrates safer and more adaptive behavior in complex scenarios. In the first corner case scenario, the ego vehicle turns right into a lane blocked by an excavator. The baseline model shows issues with understanding the scene and proceeds hesitantly, resulting in a collision with the white vehicle approaching from behind. In contrast, the distilled model anticipates the blockage and performs a swift lane change before the white car approaches. In the second corner case scenario, a white car drives on the wrong side of the road, approaching the ego. The baseline model reacts too late and causes a crash while steering into the opposing road. Our distilled model, however, avoids the collision by swiftly changing into the free lane on the right, showing a safety-oriented understanding of the scene. These results highlight that semantic distillation from LLMs equips the BEV encoder with improved situational understanding and safety awareness beyond simply imitating human trajectories in common scenarios [35]. More qualitative examples on the NeuroNCAP benchmark are given in Appendix D.

#### 5.4 Ablation Studies

**BEV Token Downsampling Method.** We conduct an ablation study to determine the optimal BEV downsampling method for the projector, with results for six variants presented in Tab. 5. Given the objective of a lightweight projector, only simple sampling methods are evaluated, supporting the hypothesis that the BEV tokens are already highly expressive and suitable for direct use. Parameter-free methods include *Avg. Pool*, *Max. Pool*, and a *Concat* operation (equiva-



(a) **Corner Case 1: Right-Turn Conflict with Blocked Lane:** In this scenario, the ego vehicle attempts to turn right at an intersection, but the rightmost lane after the turn is blocked by an excavator. Meanwhile, a vehicle traveling straight in the adjacent lane restricts the available space, requiring the ego to adjust its trajectory to avoid a potential collision.



(b) **Corner Case 2: Oncoming Car in Ego Lane:** In this scenario, the ego vehicle drives on a two-way road with two lanes in each direction. A car from the opposite direction enters the ego vehicle's lane and drives toward it on the wrong side of the road. To avoid a collision, the ego vehicle needs to move to the free right lane in its own direction.

**Fig. 4: Qualitative NeuroNCAP Results.** Two representative closed-loop planning scenarios are presented for comparison between the baseline and semantically distilled models. The distilled model demonstrates improved decision-making under safety-critical scenarios, successfully performing a *safe right turn* in corner case 1 and an *evasive lane change to the free right lane* in corner case 2 to avoid potential collisions, where the baseline model fails.

lent to a pixel unshuffle used in VLMs [81]), which substantially increases the projector's parameter count. Additionally, several learnable methods for down-sampling are assessed: a 1-layer standard *Conv*, and a more parameter-efficient *Depthw. Conv* [10]. Same as before, accuracy is measured for existence-based questions. Additionally, we employ various language metrics for a more precise evaluation of the open-ended questions. The results in Tab. 5 demonstrate that while the learnable methods perform well, they offer no significant advantage over simple pooling methods, which are parameter-free and computationally efficient. On the 8B LLM, *Avg. Pool* and *Max. Pool* achieve the same accuracy. We selected *Max. Pool* to create the results in this paper due to slightly better values on the language scores.

**Table 6: VQA Data Ablation.** We ablate the performance of the distilled BEV encoder on subsets of the DriveLM dataset. All models have similar collision rates (“CR”), allowing for comparison of the average velocity at impact for collision cases (“Avg. Imp. Vel.”). The different variants of BEV distillation significantly reduce impact velocities, resulting in higher NeuroNCAP scores. The *Behavior* and *Planning* questions help more than the *Perception* and *Prediction* questions, and the best result is achieved with all questions combined.

Method	Perception	Prediction	Behavior	Planning	L2@1s↓	L2@2s↓	L2@3s↓	avg.L2↓	CR@0.0s↓	Avg. Imp. Vel. ↓	NeuroNCAP Score↑
Baseline BEV					0.50	0.99	1.67	1.05	0.62	7.86	2.10
Distilled <sub>1B</sub> BEV	✓	✓			0.48	0.95	1.62	1.02	0.62	6.24	2.37
Distilled <sub>1B</sub> BEV			✓	✓	0.48	0.94	1.62	1.01	<b>0.60</b>	6.10	2.42
Distilled <sub>1B</sub> BEV	✓	✓	✓	✓	<b>0.46</b>	<b>0.91</b>	<b>1.55</b>	<b>0.97</b>	0.63	<b>5.36</b>	<b>2.46</b>

**Distillation VQA Data.** We further conduct an ablation study from the VQA data perspective. Specifically, we study what type of question can best benefit the BEV semantic learning by separating the questions in the DriveLM dataset, including *Perception*, *Prediction*, *Behavior*, and *Planning*. Since the different task data samples vary, we train the less frequent subset (*i.e.*, behavior and planning) for 3 epochs while training the more frequent subset (*i.e.*, perception and prediction) for one epoch to match the overall iterations (shown in Appendix Tab. 7).

The results are presented in Tab. 6. While both subsets show a substantial improvement over the baseline with no distillation, the *Behavior* and *Planning* questions give the main improvement on the NeuroNCAP score, while adding *Perception* and *Prediction* questions on top brings only 1.65% improvement.

The collision rate is similar for all variants, so the higher NeuroNCAP score indicates that the velocity at impact is much lower for the models trained from distilled BEV encoders, indicating safer and more anticipatory behavior in such corner cases. This is confirmed when comparing the average impact velocity. The UniAD baseline trained without distillation has  $7.86 \text{ m s}^{-1}$ . Training on the *Perception* and *Prediction* subset reduces the average impact velocity to  $6.24 \text{ m s}^{-1}$ . Instead, training on the *Behavior* and *Planning* subset is even more impactful, reaching  $6.10 \text{ m s}^{-1}$ . Most importantly, the distillation variant from all DriveLM questions reaches the lowest average impact velocity with  $5.36 \text{ m s}^{-1}$ , showing that both subsets complement each other. More qualitative results together with the corresponding velocity profiles are discussed in Appendix D.3.

## 6 Discussion & Conclusion

**Limitations.** In this work, we mainly use the DriveLM-nuScenes [56] dataset for the experiments. We select this dataset due to its (1) compatibility with nuScenes [5] and (2) curated and high-quality ground truth. However, this should not be a major concern, as the distillation from this dataset alone already brings significant improvement. Evaluating the distilled BEV representation on more diverse and semantically rich VQA data to confirm the scaling of the framework is left for future work. More discussion is in Appendix E.

**Conclusion.** In this work, we presented a framework that unifies the spatial structure of BEV representations with the semantic reasoning capabilities of LLMs. We show that BEV features can be effectively tokenized for LLM processing and that they enable stronger spatial reasoning than image-based tokens in multi-view settings. Building on this insight, we introduced BEVLM, which distills semantic knowledge from LLMs into BEV encoders. This semantic enrichment leads to consistent gains in end-to-end driving, including up to 29% improvement in safety on the NeuroNCAP benchmark. These results highlight the promise of integrating BEV with LLM reasoning to improve the safety and reliability of autonomous driving systems.

## 7 Acknowledgments

We thank Mukesh Ghimire and Joona Hellmuth for their help with running the NeuroNCAP closed-loop simulation.

## References

1. Achiam, J., Adler, S., Agarwal, S., Ahmad, L., Akkaya, I., Aleman, F.L., Almeida, D., Altenschmidt, J., Altman, S., Anadkat, S., et al.: GPT-4 Technical Report. arXiv preprint arXiv:2303.08774 (2023)
2. Antol, S., Agrawal, A., Lu, J., Mitchell, M., Batra, D., Zitnick, C.L., Parikh, D.: VQA: Visual Question Answering. In: Proceedings of the IEEE International Conference on Computer Vision (ICCV) (2015)
3. Banerjee, S., Lavie, A.: METEOR: An Automatic Metric for MT Evaluation with Improved Correlation with Human Judgments. In: Proceedings of the acl workshop on intrinsic and extrinsic evaluation measures for machine translation and/or summarization. pp. 65–72 (2005)
4. Brandstaetter, F., Schuetz, E., Winter, K., Flohr, F.: BEV-LLM: Leveraging Multimodal BEV Maps for Scene Captioning in Autonomous Driving. arXiv Preprint arXiv:2507.19370 (2025)
5. Caesar, H., Bankiti, V., Lang, A.H., Vora, S., Liong, V.E., Xu, Q., Krishnan, A., Pan, Y., Baldan, G., Beijbom, O.: nuScenes: A Multimodal Dataset for Autonomous Driving. In: Proceedings of the IEEE/CVF Conference on Computer Vision and Pattern Recognition (CVPR) (2020)
6. Cao, W., Hallgarten, M., Li, T., Dauner, D., Gu, X., Wang, C., Miron, Y., Aiello, M., Li, H., Gilitschenski, I., Ivanovic, B., Pavone, M., Geiger, A., Chitta, K.: Pseudo-Simulation for Autonomous Driving. In: Conference on Robot Learning (CoRL) (2025)
7. Cao, Y., Wang, N., Xiao, C., Yang, D., Fang, J., Yang, R., Chen, Q.A., Liu, M., Li, B.: Invisible for Both Camera and LiDAR: Security of Multi-Sensor Fusion Based Perception in Autonomous Driving Under Physical-World Attacks. In: IEEE Symposium on Security and Privacy (SP). pp. 176–194. IEEE (2021)
8. Chen, B., Xu, Z., Kirmani, S., Ichter, B., Sadigh, D., Guibas, L., Xia, F.: SpatialVLM: Endowing Vision-Language Models with Spatial Reasoning Capabilities. In: IEEE/CVF Conference on Computer Vision and Pattern Recognition (CVPR). pp. 14455–14465 (2024)

9. Chen, Y., Wang, Y., Zhang, Z.: DrivingGPT: Unifying Driving World Modeling and Planning with Multi-Modal Autoregressive Transformers. arXiv preprint arXiv:2412.18607 (2024)
10. Chollet, F.: Xception: Deep Learning with Depthwise Separable Convolutions. In: Proceedings of the IEEE Conference on Computer Vision and Pattern Recognition (CVPR) (2017)
11. Comanici, G., Bieber, E., Schaekermann, M., Pasupat, I., Sachdeva, N., Dhillon, I., Blistein, M., Ram, O., Zhang, D., Rosen, E., et al.: Gemini 2.5: Pushing the Frontier with Advanced Reasoning, Multimodality, Long Context, and Next Generation Agentic Capabilities. arXiv Preprint arXiv:2507.06261 (2025)
12. Dauner, D., Hallgarten, M., Geiger, A., Chitta, K.: Parting with Misconceptions About Learning-Based Vehicle Motion Planning. In: Conference on Robot Learning. pp. 1268–1281. PMLR (2023)
13. Dauner, D., Hallgarten, M., Li, T., Weng, X., Huang, Z., Yang, Z., Li, H., Gilitschenski, I., Ivanovic, B., Pavone, M., et al.: NavSim: Data-Driven Non-Reactive Autonomous Vehicle Simulation and Benchmarking. Advances in Neural Information Processing Systems **37**, 28706–28719 (2024)
14. Ding, S., Vasa, S., Ramadwar, A.: Explanation-Driven Counterfactual Testing for Faithfulness in Vision-Language Model Explanations. In: NeurIPS 2025 Workshop on Regulatable ML (2025)
15. Dosovitskiy, A.: An Image Is Worth 16x16 Words: Transformers for Image Recognition at Scale. arXiv Preprint arXiv:2010.11929 (2020)
16. Fadadu, S., Pandey, S., Hegde, D., Shi, Y., Chou, F.C., Djuric, N., Vallespi-Gonzalez, C.: Multi-View Fusion of Sensor Data for Improved Perception and Prediction in Autonomous Driving. In: Proceedings of the IEEE/CVF Winter Conference on Applications of Computer Vision (WACV) (2022)
17. Feng, B., Mei, Z., Li, B., Ost, J., Girgis, R., Majumdar, A., Heide, F.: VERDI: VLM-Embedded Reasoning for Autonomous Driving. arXiv preprint arXiv:2505.15925 (2025)
18. Fu, H., Zhang, D., Zhao, Z., Cui, J., Liang, D., Zhang, C., Zhang, D., Xie, H., Wang, B., Bai, X.: Orion: A Holistic End-to-End Autonomous Driving Framework by Vision-Language Instructed Action Generation. arXiv preprint arXiv:2503.19755 (2025)
19. Gholami, M., Rezaei, A., Weimin, Z., Mao, S., Zhou, S., Zhang, Y., Akbari, M.: Spatial Reasoning with Vision-Language Models in Ego-Centric Multi-View Scenes. arXiv preprint arXiv:2509.06266 (2025)
20. Guo, Z., Gubernatorov, K., Asfaw, S., Yagudin, Z., Tsetserukou, D.: VDT-Auto: End-to-End Autonomous Driving with VLM-Guided Diffusion Transformers. arXiv preprint arXiv:2502.20108 (2025)
21. He, K., Zhang, X., Ren, S., Sun, J.: Deep Residual Learning for Image Recognition. In: Proceedings of the IEEE Conference on Computer Vision and Pattern Recognition (CVPR) (2016)
22. Heo, B., Kim, J., Yun, S., Park, H., Kwak, N., Choi, J.Y.: A Comprehensive Overhaul of Feature Distillation. In: Proceedings of the IEEE/CVF International Conference on Computer Vision (ICCV). pp. 1921–1930 (2019)
23. Hinton, G., Vinyals, O., Dean, J.: Distilling the Knowledge in a Neural Network. arXiv preprint arXiv:1503.02531 (2015)
24. Hu, Y., Yang, J., Chen, L., Li, K., Sima, C., Zhu, X., Chai, S., Du, S., Lin, T., Wang, W., et al.: Planning-Oriented Autonomous Driving. In: IEEE/CVF Conference on Computer Vision and Pattern Recognition (CVPR) (2023)

25. Huang, J., Huang, G., Zhu, Z., Ye, Y., Du, D.: BEVDet: High-Performance Multi-Camera 3D Object Detection in Bird’s-Eye-View. arXiv Preprint arXiv:2112.11790 (2021)
26. Huang, Z., Tang, T., Chen, S., Lin, S., Jie, Z., Ma, L., Wang, G., Liang, X.: Making Large Language Models Better Planners with Reasoning-Decision Alignment. In: European Conference on Computer Vision (ECCV). Springer (2024)
27. Hwang, J.J., Xu, R., Lin, H., Hung, W.C., Ji, J., Choi, K., Huang, D., He, T., Covington, P., Sapp, B., Zhou, Y., Guo, J., Anguelov, D., Tan, M.: EMMA: End-to-End Multimodal Model for Autonomous Driving. *Transactions on Machine Learning Research* (2025), <https://openreview.net/forum?id=kH3t5lm0U8>
28. Jia, X., Yang, Z., Li, Q., Zhang, Z., Yan, J.: Bench2Drive: Towards Multi-Ability Benchmarking of Closed-Loop End-to-End Autonomous Driving. *Advances in Neural Information Processing Systems* **37**, 819–844 (2024)
29. Jiang, B., Chen, S., Liao, B., Zhang, X., Yin, W., Zhang, Q., Huang, C., Liu, W., Wang, X.: Senna: Bridging Large Vision-Language Models and End-to-End Autonomous Driving. arXiv preprint arXiv:2410.22313 (2024)
30. Jiang, B., Chen, S., Xu, Q., Liao, B., Chen, J., Zhou, H., Zhang, Q., Liu, W., Huang, C., Wang, X.: VAD: Vectorized Scene Representation for Efficient Autonomous Driving. In: IEEE/CVF International Conference on Computer Vision (ICCV) (2023)
31. Kirillov, A., Mintun, E., Ravi, N., Mao, H., Rolland, C., Gustafson, L., Xiao, T., Whitehead, S., Berg, A.C., Lo, W.Y., et al.: Segment Anything. In: IEEE/CVF International Conference on Computer Vision (ICCV) (2023)
32. Kong, L., Liu, Y., Li, X., Chen, R., Zhang, W., Ren, J., Pan, L., Chen, K., Liu, Z.: Robo3D: Towards Robust and Reliable 3D Perception Against Corruptions. In: IEEE/CVF International Conference on Computer Vision (ICCV) (2023)
33. Li, J., Li, D., Xiong, C., Hoi, S.: BLIP: Bootstrapping Language-Image Pre-Training for Unified Vision-Language Understanding and Generation. In: International Conference on Machine Learning (ICML). PMLR (2022)
34. Li, Z., Wang, W., Li, H., Xie, E., Sima, C., Lu, T., Qiao, Y., Dai, J.: BEVFormer: Learning Bird’s-Eye-View Representation from Multi-Camera Images via Spatiotemporal Transformers. In: European Conference on Computer Vision (ECCV). Springer (2022)
35. Li, Z., Yu, Z., Lan, S., Li, J., Kautz, J., Lu, T., Alvarez, J.M.: Is Ego Status All You Need for Open-Loop End-to-End Autonomous Driving? In: IEEE/CVF Conference on Computer Vision and Pattern Recognition (CVPR) (2024)
36. Liao, B., Chen, S., Wang, X., Cheng, T., Zhang, Q., Liu, W., Huang, C.: MapTR: Structured Modeling and Learning for Online Vectorized HD Map Construction. In: The Eleventh International Conference on Learning Representations (ICLR) (2023)
37. Lin, C.Y.: ROUGE: A Package for Automatic Evaluation of Summaries. In: Text Summarization Branches Out. pp. 74–81 (2004)
38. Lin, T.Y., Dollár, P., Girshick, R., He, K., Hariharan, B., Belongie, S.: Feature Pyramid Networks for Object Detection. In: Proceedings of the IEEE Conference on Computer Vision and Pattern Recognition (CVPR) (2017)
39. Liu, H., Li, C., Wu, Q., Lee, Y.J.: Visual Instruction Tuning. *Advances in Neural Information Processing Systems* **36** (2023)
40. Liu, Z., Tang, H., Amini, A., Yang, X., Mao, H., Rus, D.L., Han, S.: BEVFusion: Multi-Task Multi-Sensor Fusion with Unified Bird’s-Eye View Representation. In: 2023 IEEE International Conference on Robotics and Automation (ICRA). IEEE (2023)

41. Ljungbergh, W., Tonderski, A., Johnander, J., Caesar, H., Åström, K., Felsberg, M., Petersson, C.: NeuroNCap: Photorealistic Closed-Loop Safety Testing for Autonomous Driving. In: European Conference on Computer Vision (ECCV). Springer (2024)
42. Loshchilov, I., Hutter, F.: Decoupled Weight Decay Regularization. arXiv preprint arXiv:1711.05101 (2017)
43. Lu, H., Liu, W., Zhang, B., Wang, B., Dong, K., Liu, B., Sun, J., Ren, T., Li, Z., Yang, H., Sun, Y., Deng, C., Xu, H., Xie, Z., Ruan, C.: DeepSeek-VL: Towards Real-World Vision-Language Understanding (2024)
44. Ma, Y., Wang, T., Bai, X., Yang, H., Hou, Y., Wang, Y., Qiao, Y., Yang, R., Manocha, D., Zhu, X.: Vision-Centric BEV Perception: A Survey. IEEE Transactions on Pattern Analysis and Machine Intelligence (2024)
45. Min, C., Zhao, D., Xiao, L., Zhao, J., Xu, X., Zhu, Z., Jin, L., Li, J., Guo, Y., Xing, J., et al.: DriveWorld: 4D Pre-Trained Scene Understanding via World Models for Autonomous Driving. In: Proceedings of the IEEE/CVF Conference on Computer Vision and Pattern Recognition (CVPR) (2024)
46. Monninger, T., Anwar, M.Z., Antol, S., Staab, S., Ding, S.: AugMapNet: Improving Spatial Latent Structure via BEV Grid Augmentation for Enhanced Vectorized Online HD Map Construction. arXiv preprint arXiv:2503.13430 (2025)
47. Monninger, T., Zhang, Z., Mo, Z., Anwar, M.Z., Staab, S., Ding, S.: MapDiffusion: Generative diffusion for vectorized online hd map construction and uncertainty estimation in autonomous driving. In: 2025 IEEE/RSJ International Conference on Intelligent Robots and Systems (IROS). pp. 4099–4106. IEEE (2025)
48. Muhammad, K., Ullah, A., Lloret, J., Del Ser, J., De Albuquerque, V.H.C.: Deep Learning for Safe Autonomous Driving: Current Challenges and Future Directions. IEEE Transactions on Intelligent Transportation Systems **22**(7), 4316–4336 (2020)
49. Pan, C., Yaman, B., Nesti, T., Mallik, A., Allievi, A.G., Velipasalar, S., Ren, L.: VLP: Vision Language Planning for Autonomous Driving. In: IEEE/CVF Conference on Computer Vision and Pattern Recognition (CVPR) (2024)
50. Papineni, K., Roukos, S., Ward, T., Zhu, W.J.: BLEU: A Method for Automatic Evaluation of Machine Translation. In: Annual Meeting of the Association for Computational Linguistics. pp. 311–318 (2002)
51. Qian, T., Chen, J., Zhuo, L., Jiao, Y., Jiang, Y.G.: nuScenes-QA: A Multi-Modal Visual Question Answering Benchmark for Autonomous Driving Scenario. In: AAAI Conference on Artificial Intelligence. vol. 38, pp. 4542–4550 (2024)
52. Radford, A., Kim, J.W., Hallacy, C., Ramesh, A., Goh, G., Agarwal, S., Sastry, G., Askell, A., Mishkin, P., Clark, J., Krueger, G., Sutskever, I.: Learning Transferable Visual Models from Natural Language Supervision. In: International Conference on Machine Learning (ICML). PMLR (2021)
53. Renz, K., Chen, L., Arani, E., Sinavski, O.: SimLingo: Vision-Only Closed-Loop Autonomous Driving with Language-Action Alignment. In: IEEE/CVF Conference on Computer Vision and Pattern Recognition (CVPR). pp. 11993–12003 (2025)
54. Sato, T., Shen, J., Wang, N., Jia, Y., Lin, X., Chen, Q.A.: Dirty Road Can Attack: Security of Deep Learning Based Automated Lane Centering Under Physical-World Attack. In: 30th USENIX Security Symposium (USENIX Security) (2021)
55. Shao, H., Hu, Y., Wang, L., Song, G., Waslander, S.L., Liu, Y., Li, H.: LMDrive: Closed-Loop End-to-End Driving with Large Language Models. In: IEEE/CVF Conference on Computer Vision and Pattern Recognition (CVPR) (2024)
56. Sima, C., Renz, K., Chitta, K., Chen, L., Zhang, H., Xie, C., Beifwenger, J., Luo, P., Geiger, A., Li, H.: DriveLM: Driving with Graph Visual Question Answering. In: European Conference on Computer Vision (ECCV). Springer (2024)

57. Tian, X., Gu, J., Li, B., Liu, Y., Wang, Y., Zhao, Z., Zhan, K., Jia, P., Lang, X., Zhao, H.: DriveVLM: The Convergence of Autonomous Driving and Large Vision-Language Models. In: Conference on Robot Learning. pp. 4698–4726. PMLR (2024)
58. Vedantam, R., Zitnick, C.L., Parikh, D.: CIDEr: Consensus-Based Image Description Evaluation. In: IEEE/CVF Conference on Computer Vision and Pattern Recognition (CVPR). pp. 4566–4575 (2015)
59. Wan, Z., Shen, J., Chuang, J., Xia, X., Garcia, J., Ma, J., Chen, Q.A.: Too Afraid to Drive: Systematic Discovery of Semantic DoS Vulnerability in Autonomous Driving Planning Under Physical-World Attacks. In: ISOC Network and Distributed Systems Security (NDSS) Symposium (2022)
60. Wang, S., Yu, Z., Jiang, X., Lan, S., Shi, M., Chang, N., Kautz, J., Li, Y., Alvarez, J.M.: OmniDrive: A Holistic Vision-Language Dataset for Autonomous Driving with Counterfactual Reasoning. In: IEEE/CVF Conference on Computer Vision and Pattern Recognition (CVPR) (2025)
61. Wang, Y., Luo, W., Bai, J., Cao, Y., Che, T., Chen, K., Chen, Y., Diamond, J., Ding, Y., Ding, W., et al.: Alpamayo-R1: Bridging Reasoning and Action Prediction for Generalizable Autonomous Driving in the Long Tail. arXiv preprint arXiv:2511.00088 (2025)
62. Winter, K., Azer, M., Flohr, F.B.: BEVDriver: Leveraging BEV Maps in LLMs for Robust Closed-Loop Driving. arXiv Preprint arXiv:2503.03074 (2025)
63. Wu, P., Chen, S., Metaxas, D.N.: MotionNet: Joint Perception and Motion Prediction for Autonomous Driving Based on Bird’s Eye View Maps. In: Proceedings of the IEEE/CVF Conference on Computer Vision and Pattern Recognition (CVPR) (2020)
64. Xie, S., Kong, L., Dong, Y., Sima, C., Zhang, W., Chen, Q.A., Liu, Z., Pan, L.: Are VLMs Ready for Autonomous Driving? An Empirical Study from the Reliability, Data, and Metric Perspectives. In: IEEE/CVF International Conference on Computer Vision (ICCV) (October 2025)
65. Xie, S., Kong, L., Zhang, W., Ren, J., Pan, L., Chen, K., Liu, Z.: Benchmarking and Improving Bird’s Eye View Perception Robustness in Autonomous Driving. IEEE Transactions on Pattern Analysis and Machine Intelligence **47**(5) (2025). <https://doi.org/10.1109/TPAMI.2025.3535960>
66. Xie, S., Li, Z., Wang, Z., Xie, C.: On the Adversarial Robustness of Camera-Based 3D Object Detection. Transactions on Machine Learning Research (2024)
67. Xie, Y., Xu, R., He, T., Hwang, J.J., Luo, K., Ji, J., Lin, H., Chen, L., Lu, Y., Leng, Z., et al.: S4-Driver: Scalable Self-Supervised Driving Multimodal Large Language Model with Spatio-Temporal Visual Representation. In: IEEE/CVF Conference on Computer Vision and Pattern Recognition (CVPR) (2025)
68. Xu, Y., Hu, Y., Zhang, Z., Meyer, G.P., Mustikovela, S.K., Srinivasa, S., Wolff, E.M., Huang, X.: VLM-AD: End-to-End Autonomous Driving Through Vision-Language Model Supervision. arXiv preprint arXiv:2412.14446 (2024)
69. Xu, Z., Zhang, Y., Xie, E., Zhao, Z., Guo, Y., Wong, K.Y.K., Li, Z., Zhao, H.: DriveGPT4: Interpretable End-to-End Autonomous Driving via Large Language Model. IEEE Robotics and Automation Letters **9**(10) (2024)
70. Yang, A., Li, A., Yang, B., Zhang, B., Hui, B., Zheng, B., Yu, B., Gao, C., Huang, C., Lv, C., et al.: Qwen3 Technical Report. arXiv Preprint arXiv:2505.09388 (2025)
71. Yang, A., Yang, B., Zhang, B., Hui, B., Zheng, B., Yu, B., Li, C., Liu, D., Huang, F., Wei, H., Lin, H., Yang, J., Tu, J., Zhang, J., Yang, J., Yang, J., Zhou, J., Lin, J., Dang, K., Lu, K., Bao, K., Yang, K., Yu, L., Li, M., Xue, M., Zhang, P., Zhu, Q., Men, R., Lin, R., Li, T., Tang, T., Xia, T., Ren, X., Ren, X., Fan, Y., Su,

- Y., Zhang, Y., Wan, Y., Liu, Y., Cui, Z., Zhang, Z., Qiu, Z.: Qwen2.5 Technical Report (2025), <https://arxiv.org/abs/2412.15115>
72. Yang, H., Zhang, S., Huang, D., Wu, X., Zhu, H., He, T., Tang, S., Zhao, H., Qiu, Q., Lin, B., et al.: UniPAD: A Universal Pre-Training Paradigm for Autonomous Driving. In: Proceedings of the IEEE/CVF Conference on Computer Vision and Pattern Recognition (CVPR) (2024)
  73. Yang, Z., Jia, X., Li, H., Yan, J.: LLM4Drive: A Survey of Large Language Models for Autonomous Driving. arXiv preprint arXiv:2311.01043 (2023)
  74. Zeng, S., Chang, X., Xie, M., Liu, X., Bai, Y., Pan, Z., Xu, M., Wei, X., Guo, N.: FutureSightDrive: Thinking Visually with Spatio-Temporal COT for Autonomous Driving. arXiv preprint arXiv:2505.17685 (2025)
  75. Zhai, X., Mustafa, B., Kolesnikov, A., Beyer, L.: Sigmoid Loss for Language Image Pre-Training. In: IEEE/CVF International Conference on Computer Vision (ICCV) (2023)
  76. Zhang, Y., Zhu, Z., Zheng, W., Huang, J., Huang, G., Zhou, J., Lu, J.: BEVerse: Unified Perception and Prediction in Bird's-Eye-View for Vision-Centric Autonomous Driving. arXiv Preprint arXiv:2205.09743 (2022)
  77. Zhou, X., Liang, D., Tu, S., Chen, X., Ding, Y., Zhang, D., Tan, F., Zhao, H., Bai, X.: HERMES: A Unified Self-Driving World Model for Simultaneous 3D Scene Understanding and Generation. In: IEEE/CVF International Conference on Computer Vision (ICCV) (October 2025)
  78. Zhou, X., Han, X., Yang, F., Ma, Y., Knoll, A.C.: OpenDriveVLA: Towards End-to-End Autonomous Driving with Large Vision Language Action Model. arXiv preprint arXiv:2503.23463 (2025)
  79. Zhou, Z., Cai, T., Zhao, S.Z., Zhang, Y., Huang, Z., Zhou, B., Ma, J.: AutoVLA: A Vision-Language-Action Model for End-to-End Autonomous Driving with Adaptive Reasoning and Reinforcement Fine-Tuning. arXiv preprint arXiv:2506.13757 (2025)
  80. Zhu, D., Chen, J., Shen, X., Li, X., Elhoseiny, M.: MiniGPT-4: Enhancing Vision-Language Understanding with Advanced Large Language Models. In: The Twelfth International Conference on Learning Representations (ICLR) (2024)
  81. Zhu, J., Wang, W., Chen, Z., Liu, Z., Ye, S., Gu, L., Tian, H., Duan, Y., Su, W., Shao, J., et al.: InternVL3: Exploring Advanced Training and Test-Time Recipes for Open-Source Multimodal Models. arXiv Preprint arXiv:2504.10479 (2025)

# BEVLM: Distilling Semantic Knowledge from LLMs into Bird’s-Eye View Representations

## – Supplementary Material –

### Table of Contents

A	More Implementation Details . . . . .	21
A.1	Dataset Details . . . . .	22
	DriveLM Dataset. . . . .	22
	Ego3D Dataset. . . . .	22
A.2	Baselines Details . . . . .	23
	Majority Class. . . . .	23
	Linear Probe. . . . .	23
	Detection Baseline. . . . .	24
A.3	Visual Tokenization Implementation . . . . .	24
A.4	Implementation of BEVLM Framework . . . . .	24
	Distillation Mechanism and Setup. . . . .	24
	Coordinate Conversion. . . . .	25
A.5	Training Configurations . . . . .	25
	Training Parameters. . . . .	25
	MLP Projector Design. . . . .	25
	Data Pipeline. . . . .	26
B	More Experimental Results. . . . .	26
C	Example Text Data . . . . .	26
C.1	DriveLM Example Question-Answer Pairs . . . . .	26
C.2	Ego3D Example Question-Answer Pairs . . . . .	27
D	More Qualitative Results on NeuroNCAP . . . . .	28
D.1	More Qualitative Results . . . . .	28
D.2	Failure Cases of Distilled Model . . . . .	29
D.3	Analysis of Impact Severity . . . . .	29
E	Broader Impact and Limitations . . . . .	30
E.1	Broader Impact . . . . .	30
E.2	Limitations . . . . .	30
	BEV Model Architecture Generality. . . . .	31
	Human Labor-Free Distillation. . . . .	31
F	Public Resources Used . . . . .	31

### A More Implementation Details

In this section, we describe the detailed implementation in the main paper.

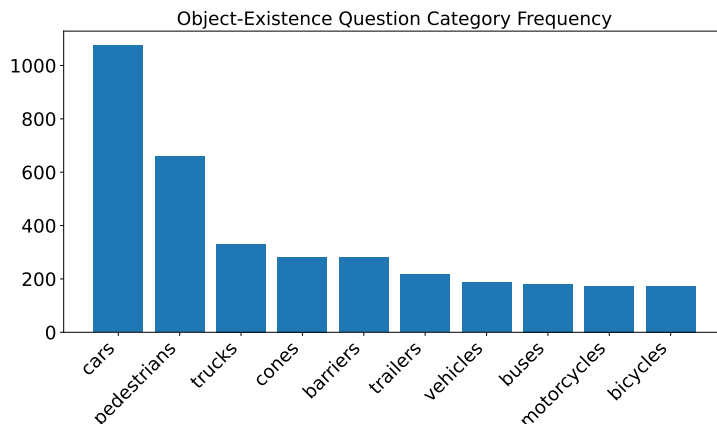


**Fig. A.1: DriveLM Dataset Object Frequency.** We visualize the object frequency in the *Perception* object-existence related questions, which are used to compute accuracy in Tab. 1 and Tab. 2 in the main paper.

### A.1 Dataset Details

**DriveLM Dataset.** The DriveLM-nuScenes [56] data distribution is shown in Tab. 7. For the results in Table 1 and 2 of the main paper, we use only the *Perception* split for training. We use the full dataset for semantic distillation in Sec. 4.

For the accuracy evaluation questions (*i.e.*, *object-existence* questions), we report the frequency of each object category in Fig. A.1. We apply filtering for these questions to ensure a fair comparison across methods. Specifically, we observe that some detection-related questions in DriveLM contain incorrect answers or reference objects located far from the ego vehicle. BEV-based models, however, are trained to represent the scene only within a limited spatial extent. For example, BEVFormer [34] and UniAD [24] use a 3D cuboid centered on the ego vehicle with range  $[-51.2, -51.2, -5.0, 51.2, 51.2, 3.0]$  along  $[-x, -y, -z, x, y, z]$  in the ego frame. Therefore, we keep the questions whose referenced ground-truth objects fall within this spatial range. We apply the same filtering to the 3D annotations before determining whether a question can be answered correctly. After filtering, 3,609 questions remain for evaluating the *object-existence* accuracy, which is reported in Tab. 1 and Tab. 2 of the main paper.

**Ego3D Dataset.** The Ego3D dataset [19] only includes the evaluation split with 2,231 pieces of data originated from the nuScenes dataset [5]. We split the dataset into training and testing sets with a ratio of 8:2. Specifically, we use 1,780 pieces of data as the training set and evaluated on the “*object-centric*” question type in the testing set, since it requires cross-view reasoning. The distribution of testing data used in Tab. 3 can be found in Tab. 8.

**Table 7: Detailed training VQA data distribution** of the DriveLM-nuScenes dataset [56]. The perception data is mainly used for Tab. 1 and Tab. 2 in the main paper, while the full set is used for semantic distillation.

Driving Task	Question Type	# Samples	Total
○ Perception	Yes-or-No & VQA	139,187	<b>298,620</b>
○ Prediction	VQA	85,842	
○ Planning	VQA	69,935	
○ Behavior	VQA	3,656	

**Table 8: Detailed Ego3D testing data distribution.**

Driving Task	Question Type	# Samples	Total
○ Localization	MCQ	43	<b>162</b>
○ Object-Centric Abs. Dist.	MCQ	42	
○ Object-Centric Rel. Dist.	MCQ	34	
○ Object-Centric Abs. Dist.	Numerical	43	

## A.2 Baselines Details

In this section, we describe how the baselines in Tab. 1 of the main paper are computed. These baselines help evaluate how well BEV features are aligned with the language space.

**Majority Class.** For this baseline, we examine the training split of the DriveLM dataset. For each *object category* (e.g., car, pedestrian), we collect all questions following the pattern “*Is there a {status} category in the {view angle}?*”, ignoring the specific *status* and *view angle*. We then count whether “Yes” or “No” appears more often for that category. During testing, for any question referring to the same object category, we always output this majority answer. This serves as a simple prior-based baseline. If a model performs similarly to this baseline, it suggests that the learned projector is mainly capturing dataset bias rather than extracting meaningful information from BEV features, as discussed in prior work [64].

**Linear Probe.** This section provides more information on the region-aware linear probe designed for the ego-centric spatial questions in DriveLM. For each question, we generate a binary spatial mask on the BEV plane corresponding to the specified camera view (e.g., "front-left"), derived from the nuScenes camera extrinsic parameters. This mask is applied element-wise to the BEV feature grid to isolate features within the relevant field of view. We employ global max pooling over the spatial dimensions of the masked features, followed by Layer Normalization. Based on the object class in the question, the resulting vector is then passed to a class-specific linear classifier to predict a binary existence

probability. This formulation serves as a baseline to isolate the representation’s semantic quality from global dataset biases while leveraging location and object information from the question.

**Detection Baseline.** We also compare BEVLM against the UniAD detection baseline [24]. This is a task-specific model that uses the same BEV encoder, so both approaches have access to the same underlying spatial information. If our projector preserves most information in BEV features, its performance should approach the detector’s performance. Following the standard UniAD setup [24], we use the detection head to predict 3D bounding boxes. For each test question, we match the question to the predicted boxes using three criteria: *object category*, *moving status*, and *view angle*.

For computing the view angle, we follow the nuScenes camera configuration [51]. The front and side cameras have a  $70^\circ$  field of view (FOV), while the rear camera has a  $110^\circ$  FOV. Therefore, we classify any object within the ego angle range  $[-35^\circ, 35^\circ]$  as being in the front view.

To determine the moving status, we follow the nuScenes definition and classify an object as “*moving*” if its absolute predicted speed exceeds  $0.2 \text{ m s}^{-1}$ .

### A.3 Visual Tokenization Implementation

For the  $I_{\text{UniAD}}$  comparison, we extract visual tokens from the lowest-resolution feature maps of the Feature Pyramid Network (FPN) [38], using the same MLP projector as for BEV features. FPN produces four spatial resolutions:  $116 \times 200$ ,  $58 \times 100$ ,  $29 \times 50$ , and  $15 \times 25$ , corresponding to the ResNet [21] stages in the top-down pathway with skip connections. We select the lowest-resolution map because its spatial size is closest to the BEV token count (about 2,500), which makes the comparison between image tokens and BEV tokens more balanced. With six camera views, this results in  $15 \times 25 \times 6 = 2,250$  visual tokens.

For the ViT-based comparison, we follow the InternVL3 preprocessing pipeline [81]. Each original  $900 \times 1600$  image is downsampled to  $450 \times 800$ , then split into two  $448 \times 448$  tiles by rounding the spatial size to the nearest multiple. We additionally enable `use_thumbnail=True`, which creates a third tile by resizing the full  $450 \times 800$  image into a single  $448 \times 448$  input. Each tile produces 256 visual tokens, giving  $256 \times 3 = 768$  tokens per camera view. With six views, the ViT setting uses  $768 \times 6 = 4,608$  visual tokens in total.

For DeepSeek-VL [43], we use the official implementation. Each image is processed by hybrid visual encoders, including SigLIP [75] for extracting high-level semantic features and SAM-B [31] for low-level cues. As a result, each image is represented by a fixed set of 576 visual tokens, independent of the input resolution. With six views, this yields  $576 \times 6 = 3,456$  tokens per scene.

### A.4 Implementation of BEVLM Framework

**Distillation Mechanism and Setup.** To align BEV features with the language space, we follow simple yet effective visual alignment strategies used in

VLMs [39, 80]. Specifically, we employ a lightweight MLP projector to map pre-trained BEV features [24] into BEV tokens. We avoid more complex architectures, such as Q-Former [33], to maintain simplicity and ensure a fair comparison with existing MLP-projector VLMs [71, 81].

For tokenization, the BEV feature grid  $\mathbf{B} \in \mathbb{R}^{H_{\text{BEV}} \times W_{\text{BEV}} \times C}$  can be viewed as a top-down image. Although each grid cell could serve as a BEV token, the native resolution (*e.g.*,  $200 \times 200$ ) yields extensive tokens. To balance spatial detail and efficiency, we downsample the grid into a compact representation. We introduce two special tokens,  $\langle \text{bev} \rangle$  and  $\langle / \text{bev} \rangle$ , to mark the BEV token sequence. During training, only the projector and these tokens are learned, while the BEV encoder and LLM remain frozen. We use standard next-token prediction conditioned on BEV tokens as the training objective:

$$\mathcal{L}(\theta) = -\mathbb{E}_{(\mathbf{q}, \mathbf{a}) \sim \mathcal{D}} \left[ \sum_{t=1}^T \log p_{\theta}(\mathbf{a}_t \mid \mathbf{B}, \mathbf{q}, \mathbf{a}_{1:t-1}) \right],$$

where  $\theta$  denotes the model parameters, and  $\mathbf{q}$  and  $\mathbf{a}$  are the question and ground-truth answer.

**Coordinate Conversion.** DriveLM dataset typically describe object locations using image-plane coordinates [56, 64], *e.g.* (450 px, 360 px). However, our approach feeds BEV tokens to the LLM, which requires reasoning in an ego-centric spatial frame. To align with this representation, we convert object locations from image coordinates to the ego-centric BEV frame, enabling more intuitive spatial reasoning. For instance, instead of expressing a location as “*Object appears at (450 px, 360 px)*”, we reformulate it as “*Object appears 3 meters in front of the ego vehicle and 1.5 meters to the left*”. This conversion is achieved by projecting the 3D ground-truth bounding boxes onto the image plane and matching them by using Intersection-over-Union (IoU), retaining only matches above a predefined threshold. For Ego3D dataset, this step is not needed since there is no coordinate-related data [19].

## A.5 Training Configurations

**Training Parameters.** For the experiments in Tab. 1 and Tab. 2 of the main paper, we train the projector for 4 epochs to ensure stable convergence. We use a learning rate of  $1 \times 10^{-3}$  with cosine learning-rate decay and the AdamW optimizer [42]. For encoder fine-tuning, we start from the trained projector and train for one additional epoch, using a learning rate of  $1 \times 10^{-5}$  for the projector and  $1 \times 10^{-6}$  for the encoder.

**MLP Projector Design.** We follow the same MLP projector design as that in the InternVL3 [81]. Specifically, the MLP projector is composed of  $\{\text{LayerNorm}, \text{Linear}, \text{GELU}, \text{Linear}\}$ , sequentially. We use the same MLP projector for BEV alignment, both for InternVL3 and DeepSeek-VL [43].

**Table 9: BEV Projector Alignment Study.** We compare the performance of three baselines with the performance of an LLM that operates directly on the BEV grid. We report accuracy individually for each class as an extension of Table 1. *Majority class* denotes using the majority choices from the training set for each category (Sec. A.2).

Models	Modality	cars	pedestrians	trucks	cones	barriers	trailers	const.	vehicles	buses	motorcycles	bicycles	Average↑
Majority class	-	92.7	81.9	65.0	59.6	54.8	66.7	83.4	75.0	79.9	77.5	78.2	78.2
Linear probe	-	94.6	87.2	84.2	83.8	83.9	95.4	87.2	85.3	84.2	84.4	88.7	88.7
Detection <sub>UniAD</sub>	-	91.1	90.9	86.7	99.0	99.6	92.6	95.7	96.1	94.8	93.6	92.8	92.8
InternVL3 <sub>1B</sub>	B <sub>UniAD</sub>	94.7	88.9	85.8	90.1	88.6	94.9	90.4	90.0	90.2	85.6	90.8	90.8
InternVL3 <sub>8B</sub>	B <sub>UniAD</sub>	97.7	94.8	89.7	94.0	95.0	97.2	92.0	96.7	96.0	94.8	95.3	95.3

**Table 10: Scene Representation Results.** We report accuracy individually for each class as an extension of Table 2. “**I**” denotes image-space representations, whereas “**B**” denotes BEV-space representations. “Proj.” indicates training only the MLP projector, while “Enc.” refers to training the modality encoder.

Models	Modality	Proj.	Enc.	cars	pedestrians	trucks	cones	barriers	trailers	const.	vehicles	buses	motorcycles	bicycles	Average↑
InternVL3 <sub>1B</sub>	I <sub>ViT</sub>			92.8	83.5	69.8	81.6	55.2	55.1	31.0	52.2	55.8	62.4	74.2	74.2
InternVL3 <sub>1B</sub>	I <sub>ViT</sub>	✓		95.7	88.6	84.3	89.7	88.3	89.4	89.8	85.0	87.4	87.9	90.3	90.3
InternVL3 <sub>1B</sub>	I <sub>ViT</sub>	✓	✓	95.5	88.8	85.2	89.4	89.0	89.8	89.8	87.8	87.4	87.9	90.5	90.5
InternVL3 <sub>1B</sub>	I <sub>UniAD</sub>	✓		94.8	89.4	82.2	89.4	89.0	94.9	89.8	83.3	82.2	84.4	89.8	89.8
InternVL3 <sub>1B</sub>	I <sub>UniAD</sub>	✓	✓	94.3	89.2	83.7	89.7	89.7	95.4	88.8	85.6	81.6	85.6	89.9	89.9
InternVL3 <sub>8B</sub>	I <sub>UniAD</sub>	✓		97.2	93.3	90.3	93.6	94.0	97.7	91.4	95.0	93.7	91.9	94.5	94.5
InternVL3 <sub>8B</sub>	I <sub>UniAD</sub>	✓	✓	97.3	93.0	89.1	91.5	94.0	97.7	94.7	94.4	94.3	92.5	94.4	94.4
InternVL3 <sub>1B</sub>	B <sub>UniAD</sub>	✓		94.7	88.9	85.8	90.1	88.6	94.9	90.4	90.0	90.2	85.6	90.8	90.8
InternVL3 <sub>1B</sub>	B <sub>UniAD</sub>	✓	✓	94.6	89.2	87.0	89.4	90.8	94.4	89.3	89.4	91.4	86.7	91.1	91.1
InternVL3 <sub>8B</sub>	B <sub>UniAD</sub>	✓		97.7	94.8	89.7	94.0	95.0	97.2	92.0	96.7	96.0	94.8	95.3	95.3
InternVL3 <sub>8B</sub>	B <sub>UniAD</sub>	✓	✓	96.8	95.3	90.3	93.3	94.7	96.3	93.6	97.8	95.4	94.8	95.2	95.2

**Data Pipeline.** We iterate over the question-answer samples while retrieving the corresponding images using the scene token defined in nuScenes [5]. Therefore, the same set of multi-view images might be used multiple times, depending on the number of questions for that specific scene.

## B More Experimental Results

We provide the full class accuracy beyond the most frequent five classes reported in the main paper (Tab. 1). The results are illustrated in Tabs. 9 and 10. The results show a similar trend that the BEV representation shows consistently better performance compared to the perspective-view representations, which further justifies our claims.

## C Example Text Data

### C.1 DriveLM Example Question-Answer Pairs

We provide examples of the *object-existence* questions, which are a subset of *Perception* questions that we use to compute the accuracy, as shown below:

**Q:** Are there moving cars to the back right of the ego car?

**A:** Yes.

**Q:** Are there barriers to the front of the ego car?

**A:** No.

**Q:** Are there traffic cones to the front left of the ego car?

**A:** No.

**Q:** Are there parked cars to the back left of the ego car?

**A:** Yes.

**Q:** Are there bicycles without riders to the front right of the ego car?

**A:** No.

**Q:** Are there standing pedestrians to the front of the ego car?

**A:** Yes.

## C.2 Ego3D Example Question-Answer Pairs

We provide examples of the testing questions in Ego3D, which require complex spatial reasoning. The four data points here represent “*Localization*”, “*Object-Centric Abs. Dist (MCQ)*”, “*Object-Centric Rel. Dist. (MCQ)*”, and “*Object-Centric Abs. Dist. (Numerical)*” shown in Tab. 8.

**Q:** The front view corresponds to the north direction. Assume the black BMW hatchback stopped at the barrier in the front view is facing north. From the perspective of the black BMW hatchback, where is the ego car located?

- A. Front
- B. Back
- C. Right
- D. Left

**A:** B

**Q:** How far, in meters, is the black BMW hatchback stopped at the barrier in the front view from the pedestrian wearing red and crossing the driveway in the front view?

- A. 36 meters
- B. 25 meters
- C. 13 meters
- D. 3 meters

**A:** C

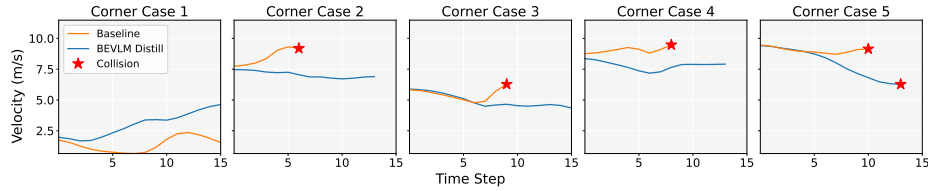


**Fig. D.1: Velocity Comparison.** We visualize the vehicle velocity for each corner case shown in the main paper and Appendix. *Case 1*: the distilled model anticipates blockage and turns swiftly to avoid the collision, while the baseline model proceeds hesitantly and collides. *Case 2*: The distilled model turns right and avoids the collision, while the baseline model speeds up and collides. *Case 3*: Speed is similar, but the distilled model turns left and successfully avoids the collision. *Case 4*: The distilled model brakes and turns to avoid collision. *Case 5 (Failure Case)*: Both models brake, but the distilled model brakes harder before the collision.

**Q:** Which one is closer to the black BMW hatchback stopped at the barrier in the front view?

- A. Ego car
- B. Pedestrian wearing red crossing the driveway

**A: A**

**Q:** How far, in meters, is the black BMW hatchback stopped at the barrier in the front view from the pedestrian wearing red and crossing the driveway in the front view?

**A: 13.7 meters**

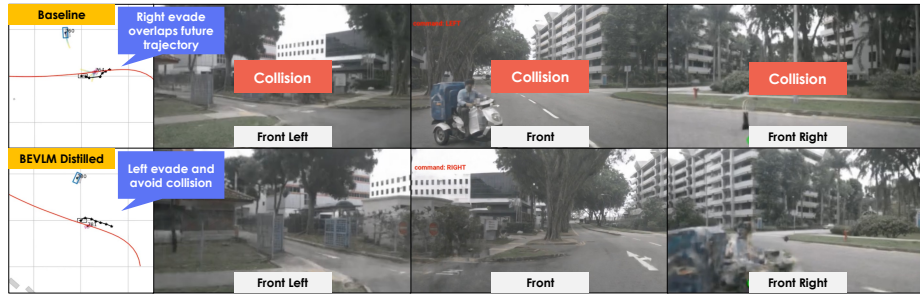
## D More Qualitative Results on NeuroNCAP

In this section, we provide and analyze further qualitative results from the NeuroNCAP corner case benchmark.

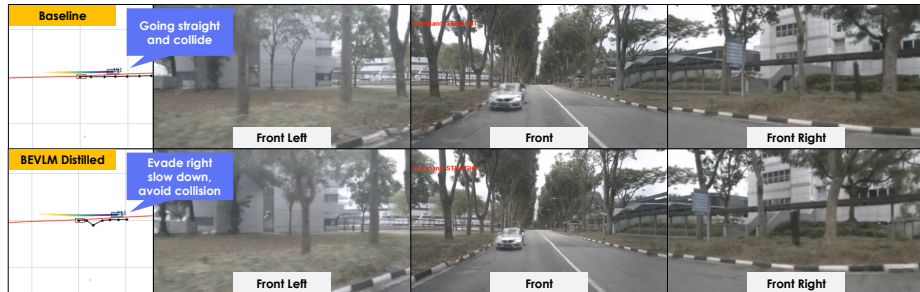
### D.1 More Qualitative Results

We present two more qualitative results in Fig. D.2. In the third corner case, the ego vehicle is moving straight while a motorcycle cuts into the lane from the left. The baseline model tries to evade by turning right, which results in a collision since it overlaps with the future trajectory of the motorcycle. In contrast, the distilled model considers the moving trajectory of the motorcycle and evades by turning left, successfully avoiding the collision.

In the fourth corner case scenario, there is a white sedan moving towards the ego vehicle in the same lane. The baseline model reacts with minimal maneuver and crashes into the oncoming car. In contrast, our distilled model reacts by turning right and slowing down to evade and prevent the collision.



(a) **Corner Case 3:** In this scenario, the ego vehicle is moving straight while a motorcycle cuts into the lane from the left. To avoid the collision, the ego vehicle is supposed to swerve to the left, avoiding the future moving trajectory of the motorcycle.



(b) **Corner Case 4:** In this scenario, a white sedan is moving towards the ego vehicle in the same lane. To avoid the collision, the ego vehicle is supposed to evade by turning right.

**Fig. D.2: Qualitative NeuroNCAP Results.** Two additional closed-loop planning scenarios are presented for comparison between the baseline and distilled models. The distilled model demonstrates improved decision-making under safety-critical scenarios, successfully performing *left evade* in corner case 3 and *right evade* in corner case 4 to avoid potential collisions, where the baseline model fails.

## D.2 Failure Cases of Distilled Model

Corner case 5 in Fig. D.3 shows a failure case of the distilled model. The challenging scenario requires evading an oncoming vehicle with an atypical appearance that drives on the wrong side of the road. The baseline UniAD model barely reacts and has a full frontal collision. Our distilled model cannot avoid the collision either, but it reacts earlier by braking and steering to the right, resulting in stronger lane deviation and lower collision impact. The contrast is particularly visible in the velocity profile in Fig. D.1, where the baseline keeps its velocity, while our distilled model reduces its velocity by around 35%, reducing the kinetic energy by more than half.

## D.3 Analysis of Impact Severity

We also visualize the ego vehicle speed at each scenario in the main paper and in the Appendix, shown in Fig. D.1. The distilled model shows an obvious trend

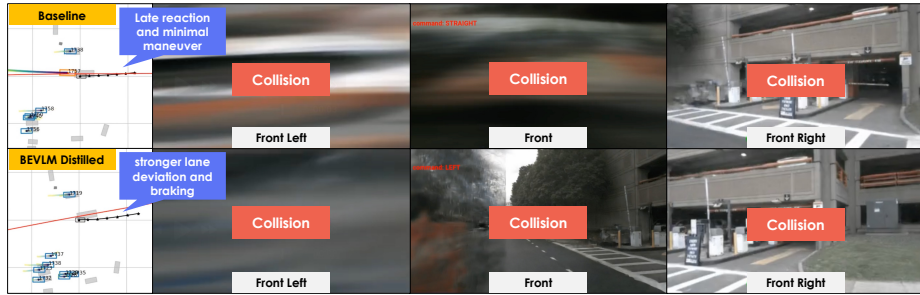


**Fig. D.3: Corner Case 5 (Failure Case).** Both the distilled model and the baseline model crash in this challenging scenario. However, our distilled model initiates the evasive maneuver much earlier, deviating more strongly from the lane center at impact time. As shown in the velocity profile in Fig. D.1, it also starts braking early, showing better safety awareness in this failure case.

of slowing down under all the scenarios except case 1 (*i.e.*, Fig. 4a in the main paper). For case 1, the distilled model anticipates the blockage and turns swiftly before another vehicle approaching from behind, while the baseline model proceeds hesitantly and eventually collides. For other cases, the baseline model shows little safety awareness and maintains the speed even before a collision. In the final cases, even when both models collide with the truck, the distilled model brakes harder before the collision, leading to a lower collision severity.

## E Broader Impact and Limitations

In this section, we discuss the broader implications of our study and acknowledge its potential limitations.

### E.1 Broader Impact

We demonstrate the potential of BEV representation to enable better spatial reasoning in autonomous driving. While most of our evaluation focuses on end-to-end driving with conventional pipelines (*e.g.*, UniAD [24]), we hope this can provide insights into designing BEV-based VLAs that enhance the spatial reasoning capability while also benefiting from the semantic knowledge needed for reasoning in corner cases.

### E.2 Limitations

In this subsection, we discuss the limitations of our work, which are mainly caused by the heavy computational costs. Additionally, we provide justification of why the main contribution of this work is still valid, given these limitations.

**BEV Model Architecture Generality.** We conducted our primary experiments using the BEV encoder architecture initially proposed in BEVFormer [34] and subsequently adopted by UniAD [24]. This choice is motivated by the fact that several representative end-to-end autonomous driving models are built upon this common BEV encoder architecture, often differing only in their task-specific decoder heads [30]. Moreover, our proposed framework does not constrain the BEV architecture design as long as the intermediate BEV representation can be generated.

Meanwhile, we acknowledge the importance of demonstrating the generality of our proposed framework by experimenting with alternative BEV encoder architectures. However, conducting such experiments is constrained by the significant computational resources required. The semantic distillation step alone takes approximately 100 hours using 8 NVIDIA A100 80GB GPUs for the 8B LLMs. The subsequent end-to-end model training requires an additional 115 hours on the same hardware setup. Given this high computational cost, we must defer the exploration of other BEV architectures to future work, to demonstrate the broad applicability of our representation studies and the BEVLM framework.

**Human Labor-Free Distillation.** We recognize the current limitation: the demonstrated safety improvement is primarily based on a human-curated dataset. The main focus of this paper is the rigorous comparison of visual representations and the introduction of the semantic distillation framework itself. We note that generating high-quality pseudo-labels is a non-trivial process, requiring careful question design, data filtering, and extensive inference resources from large-scale VLMs. Therefore, to prioritize the core framework’s contribution, we regard exploring unsupervised, human-labor-free semantic distillation for future work.

## F Public Resources Used

In this section, we acknowledge the use of the following public resources during the course of this work:

- nuScenes<sup>3</sup> ..... CC BY-NC-SA 4.0
- nuScenes-devkit<sup>4</sup> ..... Apache License 2.0
- NeuroNCAP<sup>5</sup> ..... MIT License
- DriveLM<sup>6</sup> ..... Apache License 2.0
- DriveBench<sup>7</sup> ..... Apache License 2.0
- UniAD<sup>8</sup> ..... Apache License 2.0

<sup>3</sup> <https://www.nuscenes.org/nuscenes>

<sup>4</sup> <https://github.com/nutonomy/nuscenes-devkit>

<sup>5</sup> <https://github.com/atonderski/neuro-ncap>

<sup>6</sup> <https://github.com/OpenDriveLab/DriveLM>

<sup>7</sup> <https://github.com/worldbench/drivebench>

<sup>8</sup> <https://github.com/OpenDriveLab/UniAD>

- BEVFormer<sup>9</sup> ..... Apache License 2.0
- DeepSeek-VL Codebase<sup>10</sup> ..... MIT License
- DeepSeek-VL Model<sup>11</sup> ..... DeepSeek License
- InternVL3<sup>12</sup> ..... MIT License
- Ego3D<sup>13</sup> ..... No License Available

---

<sup>9</sup> <https://github.com/fundamentalvision/BEVFormer>

<sup>10</sup> <https://github.com/deepseek-ai/DeepSeek-VL>

<sup>11</sup> <https://huggingface.co/deepseek-ai/deepseek-vl-1.3b-chat>

<sup>12</sup> <https://huggingface.co/OpenGVLab/InternVL3-1B>

<sup>13</sup> <https://github.com/vbdi/Ego3D-Bench>